Experimental higher-order interference in a nonlinear triple slit

Peter Namdar,[1] Philipp K. Jenke [●],[1] Irati Alonso Calafell,[1] Alessandro Trenti [●],[1,2] Milan Radonjić,[3,4,5] Borivoje Dakić [●],[1,6] Philip Walther [●],[1,7] and Lee A. Rozema [●][1]

[1]*Faculty of Physics, University of Vienna, Vienna Center for Quantum Science and Technology (VCQ) and Research Platform for Testing the Quantum and Gravity Interface (TURIS), Boltzmanngasse 5, Vienna A-1090, Austria*

[2]*Security and Communication Technologies, Center for Digital Safety and Security, AIT Austrian Institute of Technology GmbH, Giefinggasse 4, 1210 Vienna, Austria*

[3]*Institute of Theoretical Physics, University of Hamburg, Notkestrasse 9-11, 22607 Hamburg, Germany*

[4]*Department of Physics and Research Center OPTIMAS, Rheinland-Pfälzische Technische Universität Kaiserslautern-Landau, Erwin-Schroedinger-Strasse 46, 67663 Kaiserslautern, Germany*

[5]*Institute of Physics Belgrade, University of Belgrade, Pregrevica 118, 11080 Belgrade, Serbia*

[6]*Institute for Quantum Optics and Quantum Information (IQOQI), Austrian Academy of Sciences, Boltzmanngasse 3, A-1090 Vienna, Austria*

[7]*Christian Doppler Laboratory for Photonic Quantum Computer, Faculty of Physics, University of Vienna, Boltzmanngasse 5, Vienna A-1090, Austria*

Interference between two waves is a well-known concept in physics, and its generalization to more than two waves is straightforward. The order of interference is defined as the number of paths that interfere in a manner that cannot be reduced to patterns of a lower order. In practice, second-order interference means that in, say, a triple-slit experiment, the interference pattern when all three slits are open can be predicted from the interference patterns between all possible pairs of slits. Quantum mechanics is often said to only exhibit second-order interference. However, this is only true under specific assumptions, typically single particles undergoing linear evolution. Here we experimentally show that nonlinear evolution can in fact lead to higher-order interference. The higher-order interference in our experiment can be understood using a simple classical or quantum description, namely optical coherent states interacting in a nonlinear medium. Our work shows that nonlinear evolution could open a loophole for experiments attempting to verify Born's rule by ruling out higher-order interference.

I. INTRODUCTION

Interference between particles is one of the defining phenomena of quantum mechanics, and perhaps no scenario exemplifies this better than the double-slit experiment. Although the double slit was originally used to demonstrate the wave nature of light, Feynman later famously said that it "has in it the heart of quantum mechanics" [1]. According to standard quantum theory, when one adds additional slits, a measurement of all combinations of double-slit configurations should allow one to predict the final multislit interference pattern [2]. More generally, all interference is reducible to double-slit interference. For this reason, quantum theory is said to exhibit only *second-order* interference. Thus, the number of interfering slits (or states) is distinct from the order of the interference. Sorkin introduced a measurable parameter to determine deviations from this second-order interference [2], known as the Sorkin-parameter. Finding a nonzero Sorkin-parameter would generally be understood to indicate that our standard formulation of quantum theory, based on Born's rule, is incomplete, or equivalently that nature requires a description involving higher-order interference.

Experiments finding a zero value for the Sorkin-parameter have already been carried out using a variety of physical systems [3–12]. However, in spite of these experiments, it has been shown that under certain circumstances higher-order interference can appear. In other words, operationally, quantum mechanics exhibits second-order interference only under specific assumptions. If these are violated, one can obtain a nonzero Sorkin parameter within quantum theory. To our knowledge, there are currently three mechanisms that are predicted to lead to higher-order interference within quantum theory: (i) near-field "looped" paths [13–16], (ii) multiparticle interference together with coincidence measurements [17,18], and (iii) nonlinear evolution [19]. Note that by nonlinear evolution, we refer to Hamiltonians that are nonquadratic in canonical variables, which is the case for optical nonlinearities or particle-particle interactions. Under typical conditions these effects are small, and extra effort is required to measure these deviations. Nonetheless, recent experiments have verified that looped paths [20,21] and multiparticle interference [6] can lead to higher-order interference.

In this paper, we present an experiment demonstrating that nonlinear evolution can lead to higher-order interference. We achieve this in a "nonlinear triple slit," which is composed of three laser beams interacting in an optically nonlinear crystal. We further show that, when the nonlinearity is turned off, the higher-order interference disappears. The higher-order interference we observe here is distinct from previous observations [6,20,21]. In all of those experiments, one can still apply Born's rule using linear superpositions of the *input* states. The higher-order interference in the looped-path work [20,21]

arises because the looped paths act as different input states (or slits), which are not included in the evaluation of the Sorkin parameter, while the multiparticle interference work [6] comes from the use of coincidence detection after the interference and can again be explained by linear superpositions of the input states and this detection scheme. Instead, in our work, because of the nonlinear evolution, one cannot compute the final probabilities using *linear* superpositions of the input states. One can still apply Born's rule in our experiment, but only by using linear superpositions of the *output* states. Because of this, the higher-order interference we observe is not a "post-quantum" effect, as discussed in [2,22–24], but it is rather an effect arising in the same sort of apparatus proposed in [2], but in a different parameter regime. Just as the higher-order interference observed in [20,21], our results can be described equally well with a classical or a quantum model.

II. HIGHER-ORDER INTERFERENCE

In quantum mechanics, every quantum particle can be described by a wave function ψ that is related to the probability of the outcome of a measurement, given by Born's rule as $P(x, t) = |\psi(x, t)|^2$. As a direct consequence of this and the superposition principle, the interference pattern of the double-slit experiment can be described as

$$P_{12}(x, t) = |\psi_1(x, t) + \psi_2(x, t)|^2$$
$$= \underbrace{|\psi_1|^2}_{P_1} + \underbrace{|\psi_2|^2}_{P_2} + \underbrace{\psi_1^* \psi_2 + \psi_1 \psi_2^*}_{I_{12}}, \quad (1)$$

where $\psi_k(x, t)$ are the single-slit wave functions, and we have dropped the explicit position and time dependence in the second line. In Eq. (1), P_k are the distributions attributed to the single slits and I_{12} is the interference term.

The situation is similar in a triple-slit experiment, where the interference pattern can now be described by

$$P_{123} = P_1 + P_2 + P_3 + I_{12} + I_{13} + I_{23}. \quad (2)$$

Here, P_i are the probabilities to detect a particle with only slit i open, and I_{ij} is the interference term between slits i and j, defined in Eq. (1). Strikingly, there is no third-order interference term; i.e., the interference is reducible to combinations of two-path interference patterns. To check for the validity of this formalism, the Sorkin-parameter was introduced, which can be derived directly from Eq. (2), by rewriting the interference terms as $I_{jk} = P_{jk} - P_j - P_k$ and moving all terms to the left-hand side of the equation [3]:

$$\kappa = P_{123} - P_{12} - P_{23} - P_{13} + P_1 + P_2 + P_3 - P_0, \quad (3)$$

where we have included the term P_0— the probability to observe a detection event with all slits closed—to account for experimental background. κ can be experimentally determined using the apparatus presented in Fig. 1(a). For example, P_{12} is the probability to detect a photon (at a given location) when slits 1 and 2 are open. Assuming linear evolution and single-particle states, standard quantum theory based on Born's rule predicts $\kappa = 0$ [2].

Following this, the Sorkin-parameter κ was experimentally proven to vanish within experimental error in a variety
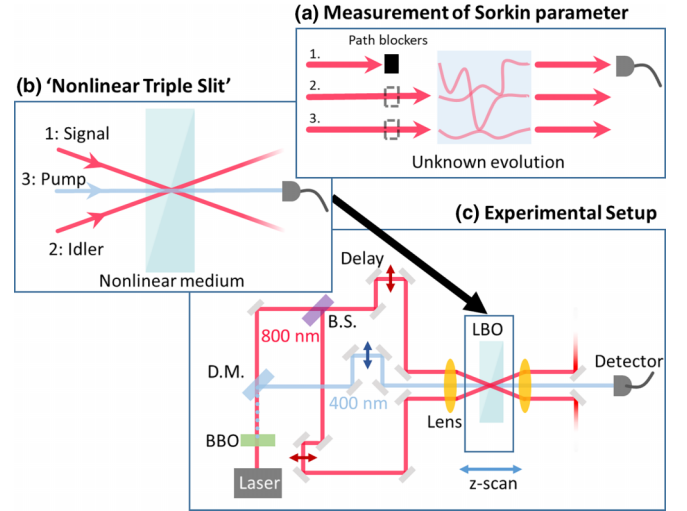

FIG. 1. (a) Measurement of the Sorkin parameter: The generic method to measure the Sorkin parameter, on some unknown evolution. Three (or more) paths are sent through the apparatus, and all combinations of paths are blocked and unblocked using the path blockers. A detector placed in a path after the process is used to estimate the probability to detect a particle. From these measurements, the Sorkin parameter is constructed using Eq. (3) from the main text. A measurement of the term P_{23} is pictured. (b) Nonlinear triple slit: A pump beam of wavelength λ interacts with a signal and an idler beam, both with wavelength 2λ in a $\chi^{(2)}$-nonlinear crystal. (c) Experimental setup: A Ti:sapphire laser emits light of $\lambda = 800$ nm with ≈ 140 fs pulses. The light is partly converted by second-harmonic generation in a beta barium borate (BBO) crystal (3 mm length, cut for type-I phase matching) to $\lambda = 400$ nm. After being separated by a dichroic mirror, the remaining fundamental beam is split into the signal and idler beams at a 50:50 beamsplitter (B.S.). The length of the beam paths can be adjusted by delay stages to ensure temporal overlap. Shutters are used to block and unblock the individual beams. The three beams are then focused into a lithium triborat (LBO) crystal (1 mm, cut for type-I phase matching). The LBO crystal is mounted on a translation stage to scan it through the focus (z-scan). This simultaneously scans the relative phase between the beams and modulates the strength of the nonlinear interaction. A photodiode after the crystal is used to measure the optical power in the pump mode.

of physical systems by measuring each individual term of Eq. (3) [3–10,20,21,25]. Most of these experiments fit the single-particle assumption of Ref. [2]. However, several used multiparticle coherent or thermal states [3–5,8–10], and, nevertheless, found $\kappa = 0$. This is likely because there was no appreciable nonlinear evolution involved. Other proposed systems, such as Bose-Einstein condensates (BECs) [26], may be more prone to nonlinear evolution. However, detector nonlinearity was noted to be present in Ref. [25] and was identified as a systematic error leading to $\kappa \neq 0$. The nonlinear detection discussed in Ref. [25] is a systematic nonlinearity (arising from nonideal detectors missing some detection events at high count rates) rather than one arising from a nonlinear Hamiltonian in the sense considered here and in Ref. [19]. If one carries out the straightforward quantum optics calculation using single-photon input states, one finds $\kappa = 0$ even in the presence of a detector nonlinearity unless multiparticle input

states are used [19]. However, the systematic nonlinearity presented in Ref. [25] shows $\kappa \neq 0$ even for single photons.

Our goal here is to experimentally determine third-order interference based on the evolution of quantum states under a nonlinear Hamiltonian. To understand how nonlinear evolution can lead to higher-order interference, consider three beams (two at frequency ω, labeled signal and idler, and a 2ω pump beam) incident on the nonlinear triple slit presented in Fig. 1(b). Although this setup differs from the first slit-based interferometers used to measure the Sorkin parameter [3], it is essentially a nonlinear interferometer [27], which are often used to enhance phase sensitivity. Furthermore, although our results do not specifically require quantum effects, it has been shown that such experiments can maintain quantum signatures [28,29]. In any case, the Sorkin parameter can be measured on any set of three or more interfering modes [19,25]. One could measure κ with any of the output beams, but we will focus only on measurements of the pump beam after the nonlinear crystal. In this case, the single path terms of Eq. (3) are easy to evaluate: $P_1 = P_2 = 0$, since the detector is mode 3, and in order to measure P_1 or P_2 light is only sent into mode 1 or 2, respectively. With light only incident in one mode, there is no mechanism to mix the modes and generate light in mode 3. (Experimentally, of course, one cannot make this assumption and must measure P_1, P_2, and P_3 directly.) Similarly, $P_3 = \mathcal{P}_{\text{pump}}/\mathcal{P}_{\text{total}}$, which is the input pump power normalized to the total input power, where $\mathcal{P}_{\text{total}} = \mathcal{P}_{\text{signal}} + \mathcal{P}_{\text{idler}} + \mathcal{P}_{\text{pump}}$, and $\mathcal{P}_{\text{signal}}$, $\mathcal{P}_{\text{idler}}$, and $\mathcal{P}_{\text{pump}}$ are the powers input into each mode. We should comment that this scenario is slightly different from "standard" experiments testing Born's rule based on interference over continuous variables–e.g., an n-slit interference pattern projected on a screen. This is because we use three discrete (approximately single-mode) optical beams in place of three slits. This single-mode approach was noted to decrease systematic errors in the measurement of κ [25] and removes essentially any contribution from looped trajectories.

The two-path terms in our work correspond to sending light into just two input modes. For example, P_{12} corresponds to sending no light in mode 3, i.e., blocking the pump. Nevertheless, light can now be generated in the pump mode via sum-frequency generation (SFG) between signal and idler [20]. Thus $P_{12} = \mathcal{P}_{\text{SFG}}/\mathcal{P}_{\text{total}}$, where $\mathcal{P}_{\text{SFG}}$ is the SFG power generated via the nonlinear mixing in the crystal. For P_{13} (P_{23}), the idler (signal) beam is blocked, and difference-frequency generation (DFG) can occur between the pump and the signal (idler) beams. We will assume the process is symmetric so $P_{13} = P_{23} = (\mathcal{P}_{\text{pump}} - \mathcal{P}_{\text{DFG}})/\mathcal{P}_{\text{total}}$. We only make these assumptions for the simple example presented here. For all of the measurements to be presented shortly, we measure each term of Eq. (3).

The final term is P_{123}, which is the power measured in mode 3 when all three beams are open. In this setting, both SFG and the two DFG processes will take place, so the three-slit term becomes $P_{123} = (\mathcal{P}_{\text{pump}} - 2\mathcal{P}'_{\text{DFG}} + \mathcal{P}'_{\text{SFG}})/\mathcal{P}_{\text{total}}$. Here $\mathcal{P}'$ denotes the fact that the conversion efficiency with all three beams open will be different from the situations with just two beams present. This can arise for two reasons. First, the various nonlinear processes modify the power in the different modes as they propagate through the crystal leading to different net conversion efficiencies.

Second, as we show in the Appendix, when one or two beams are incident, the nonlinear interactions in the crystal are independent of the relative phase. However, the nonlinear interaction between three beams is sensitive to the relative phases, leading to fundamentally different behavior between the three-path and two-path terms. This phase dependence arises because when only two beams are incident, the relative phase becomes a global phase on the excited nonlinear polarization; on the other hand, the phases do not factor out for three incident beams [see the Appendix, Eq. (A1)]. With this in mind, we can write the Sorkin parameter as

$$\kappa = [(\mathcal{P}'_{\text{SFG}} - \mathcal{P}_{\text{SFG}}) - 2(\mathcal{P}'_{\text{DFG}} - \mathcal{P}_{\text{DFG}})]/\mathcal{P}_{\text{total}}. \tag{4}$$

When the nonlinearity is small, for example in the undepleted pump regime, $\mathcal{P}'_{\text{SFG}} = \mathcal{P}_{\text{SFG}}$ and $\mathcal{P}'_{\text{DFG}} = \mathcal{P}_{\text{DFG}}$ so $\kappa = 0$. For an experimental test of higher-order interference, Eq. (3), rather than Eq. (4), should be used so as not to make any assumptions about the underlying process. Given the complex nature of the nonlinear interaction, we do not provide explicit forms of DFG and SFG interaction here, but they can be found in our MATHEMATICA code available at [30].

III. EXPERIMENT

To maximize the nonlinear interaction in our experiment, we use femtosecond pulsed beams, two of which are depicted as red ($\lambda = 800$ nm) in Fig. 1 and one is blue ($\lambda = 400$ nm) in Fig. 1. We call these three beams signal (path 1), idler (path 2), and pump (path 3), which, unless otherwise stated, have powers of approximately 870, 600, and 345 mW, respectively. As shown in Fig. 1(c), the three beams, which are generated from a single Ti:sapphire laser, are guided towards the main crystal of our setup and are spatially and temporally overlapped in a 1-mm-thick lithium triborat (LBO) crystal cut for type-I phase-matching. To satisfy the phase-matching condition, the pump beam is polarized orthogonally to the signal and idler beams. The beams are focused into the crystal with an $f = 25$ mm lens, resulting in beam waists of $\approx 30\,\mu$m. Finally, the crystal is mounted on a translation stage which can move it in and out of the focus. We use this to effectively turn on and off the nonlinear interaction. When the crystal is not in the focus (the Rayleigh range for our beams is ≈ 3 mm, and the crystal is 1 mm long), the intensities are too low to generate a measurable nonlinear response.

We will now describe our experimental procedure. To quickly set the individual configurations and measure the corresponding probabilities [as in Fig. 1(a)], we block various combinations of beams using fast (≈ 100 ms) optical shutters. The measurements are performed with a standard optical power meter, measuring the pump beam after the crystal. For each power measurement, we in fact measure the power 500 times and average the results; as shown in the Appendix (Fig. 10), this averages out the fast fluctuations. A single cycle of the experiment, measuring the power for each of the eight configurations [i.e., the individual terms of Eq. (3)], takes ≈ 1 min. To vary the strength of the nonlinear interaction, we then translate the crystal from a position behind the common focal point of the beams, through the focus, and then out of focus in front of the beams as in Ref. [31]. In absolute numbers, this corresponds to moving the crystal
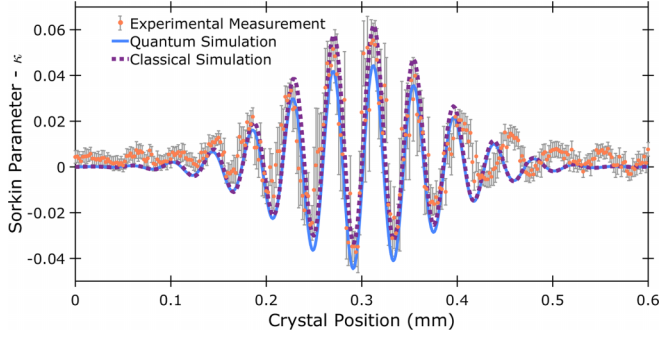
FIG. 2. Experimentally measured Sorkin-parameter vs the position of the crystal. The orange points are the experimental data. The error bars come from the standard deviation of repeated measurements of the power. The solid blue curve is the fit from the quantum model of our experiment, while the dashed violet curve is the fit generated by the classical model of our experiment.

from $z = 0.00$ to 0.60 mm, with the focus at $z \approx 0.35$ mm; the result of this measurement is plotted in Fig. 2.

In addition to varying the strength of the nonlinear interaction, this procedure induces a relative phase between the beams (as we describe in detail in the Appendix). This phase only affects the P_{123} term, and is the origin of the fringes in Fig. 2. This again shows that the higher-order interference pattern with all three slits open is qualitatively different from the second-order interference patterns. Given the phase dependence of this term, we perform additional stability measurements (Fig. 9 of the Appendix), finding that our setup is passively phase-stable for over 90 min.

A. Quantum model

To model our experiment, we use a classical and a quantum method, both of which are detailed in the Appendix. We will first present our quantum approach. We start with the Hamiltonian

$$\hat{H} = \hbar\omega\hat{a}_1^\dagger\hat{a}_1 + \hbar\omega\hat{a}_2^\dagger\hat{a}_2 + 2\hbar\omega\hat{a}_3^\dagger\hat{a}_3$$
$$+ i\hbar\chi^{(2)}(\hat{a}_1\hat{a}_2\hat{a}_3^\dagger - \hat{a}_1^\dagger\hat{a}_2^\dagger\hat{a}_3) \quad (5)$$

and we assume that coherent states $|\alpha_1\rangle_\omega$, $|\alpha_2\rangle_\omega$, and $|\alpha_3\rangle_{2\omega}$ are input into the various modes. We then apply fourth-order perturbation theory [32], and we compute the average photon number in mode 3 $\langle\hat{n}_3\rangle$ after the interaction. As shown in the Appendix, after approximating to small intersection angles we arrive at the following expression for the Sorkin parameter:

$$\kappa(Z) \approx 2\Gamma\sqrt{n_1 n_2 n_3}\, e^{-\frac{Z^2}{2\Delta^2}} \cos\left(\frac{2\pi n\theta^2}{\lambda_{1,2}}Z\right), \quad (6)$$

where n_i are the number of photons per pulse in mode i, Z is position of the crystal, θ is the angle of intersection between the pump beam and the signal (or idler) beam, $\lambda_{1,2} = 800$ nm, $n = 1.611$ is the refractive index of the LBO crystal, $\Gamma = \tau\chi^{(2)}$ is the effective nonlinear strength (given by the product of the nonlinearity and the interaction time), and Δ is an effective overlap length between the three beams. Note that the Gaussian factor in Eq. (6) is inserted by hand to model the overlap of the three beams within the nonlinear crystal.

We use the experimentally measured SFG conversion efficiencies to estimate $\Gamma = 1.05 \times 10^{-6}$ (see Fig. 6 of the Appendix). A slightly smaller value of $\Gamma = 0.525 \times 10^{-6}$ fits our data better, which likely comes from a nonideal overlap of all three beams in the crystal. The effective interaction length, $\Delta = 0.08$ mm, is set by examining the individual SFG and DFG processes as the crystal is translated through the focus. In the Appendix (Fig. 5), we observe that the nonlinear mixing is strongest when the crystal is in the focus and then rapidly decreases. For simplicity, we fix the width of the interaction region in our simulation to the narrowest process. The remaining parameter in Eq. (6) is the intersection angle θ, which is nominally $3°$ (given by the phase-matching conditions). However, we find a better fit to our data with $6.2°$. This deviation likely comes from the large numerical aperture of our focusing lens. The resulting simulation is plotted as the solid line in Fig. 2. We observe good agreement between our experimentally measured Sorkin parameter and that simulated by our model.

B. Classical model

To fit to the data with the classical model, we numerically solve the coupled wave equations governing the interaction of three beams in a nonlinear crystal [20]. In more detail, assuming collinear propagation, perfect phase-matching $\Delta k = k_1 + k_2 - k_3 = 0$, and degenerate signal and idler wavelengths $\omega_1 = \omega_2 = \frac{1}{2}\omega_3$, we can write the coupled-wave equations as

$$\frac{dE_1}{dz} = igE_3 E_2^*, \quad (7)$$

$$\frac{dE_2}{dz} = igE_3 E_1^*, \quad (8)$$

$$\frac{dE_3}{dz} = i2gE_1 E_2, \quad (9)$$

where $g = \frac{2d_{\text{eff}}\omega_1}{c}$, and d_{eff} is the nonlinear strength of the crystal. The different processes can have different efficiencies, because, for example, beams 1 and 2 may spatially and temporally overlap differently from beams 2 and 3. We thus use a different coupling constant for each differential equation:

$$\frac{dE_1}{dz} = ig_1(Z)E_3 E_2^*, \quad (10)$$

$$\frac{dE_2}{dz} = ig_2(Z)E_3 E_1^*, \quad (11)$$

$$\frac{dE_3}{dz} = i2g_3(Z)E_1 E_2. \quad (12)$$

To model translating the crystal through the focus, we further make them depend on the crystal position Z:

$$g_i(Z) = \eta_i g e^{-\frac{Z^2}{2\Delta^2}}, \quad (13)$$

where Δ characterizes the interaction range, g is a coupling constant defined above, and η_i is a fitting parameter we use to account for experimental imperfections such as beam overlap and walk-off in the crystal.

We then numerically solve these Eqs. (7)–(9) for different values of Z using MATLAB. Our code is available at [30]. In
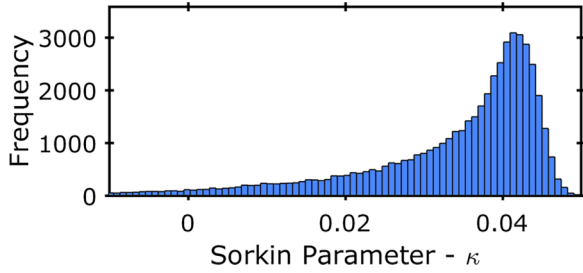
FIG. 3. A histogram of 50 000 repeated measurements of the Sorkin parameter at a fixed crystal position. For these data, the crystal was set to a position corresponding to a maximal value of κ. The asymmetric distribution occurs because phase fluctuations can only reduce this value. The net measurement time for these data was approximately 1 h.

the Appendix, we discuss the exact details of how we fit this model to our experimental data. In brief, we measure the DFG and SFG output powers for each pair of beams and fit to these using different coupling constants η_i, as illustrated in Fig. 5 of the Appendix. After fixing these parameters, the only remaining free parameters are the angle at which the beams intersect in the crystal and the interaction length, which we take to be $\theta = 6.2°$ and $\Delta = 0.08$ mm, the same as in the quantum fit to our data. The result is plotted as the dashed violet curve in Fig. 2.

IV. RESULTS AND DISCUSSION

Both our quantum and classical theoretical models, together with our experimental data, clearly show the presence of higher-order interference, without requiring any exotic physics. To better quantify this effect, we performed a longer measurement with the crystal set to the point at which we observed a maximum κ ($Z \approx 0.31$ cm). We again measured the individual terms of Eq. (3) by blocking and unblocking each of the beam paths 100 times and measuring the power; this is intended to average out any longer-term drifts. Since for each power measurement we measured the power 500 times (to average out fast drifts), this results in 50 000 individual measurements of κ in ≈ 1 h. A histogram of the observed values is shown in Fig. 3. The asymmetric distribution is due to phase fluctuations that occurred during the long measurement time. Since the experiment was aligned at a maximum of the fringe, fluctuations predominately decrease κ. To obtain our final value, we do not use the data presented in Fig. 3, since this always uses the first measured values of power to compute a value for κ, and there is no *a priori* reason to make this assumption. Instead, we estimate each term of Eq. (3) directly by taking the mean of the data presented in Fig. 7 in the Appendix. We also compute the standard error from the standard deviation of these data, and we arrive at $\kappa = 0.0334 \pm 0.0002$, where the final error bar is obtained by standard propagation of error through Eq. (3). In our definition of κ we normalize only to the input power, and not to the second-order interference ($P_{12} + P_{13} + P_{23}$), as was originally done in Ref. [3] and subsequently in several other works. Doing so would in fact slightly increase our experimentally measured κ, but, since in our experiment the relative phase

and the strength of the nonlinearity are coupled via the crystal position, this normalization complicates the analysis.

To conclude, in this paper we have presented an experiment wherein we can turn on and off higher-order interference by modulating the nonlinear interactions in our system. Together with Ref. [19], this demonstrates that multiparticle input states on their own are not sufficient to observe higher-order interference, rather nonlinearity is the key. Since many experiments searching for violations of Born's rule have used multiparticle states, our work shows that such tests must also consider sources of nonlinearities before claiming any deviation from quantum theory. Finally, we stress again that our work does not imply a failing of Born's rule. One could, of course, still apply Born's rule to our experiment. To do so, one needs to compute the quantum state *after* the nonlinear interaction, which cannot be constructed by taking a linear superposition of the states in the input modes.

APPENDIX

1. Phase induced during Z-scan

To acquire our data, we translate the crystal parallel to the pump beam through the focus. We refer to the crystal position as Z. In addition to modulating the strength of the nonlinear interaction, this induces a phase between the pump beam and the signal and idler beams. The phase is symmetric, i.e., the induced phase between the pump and signal is the same as the induced phase between the pump and idler. This effect, for the signal and pump beams, is illustrated in Fig. 4. Panel (a) shows the situation when the two beams intersect before the crystal. We define this as our 0 phase reference. As the crystal is moved through the focus, the optical path that the pump experiences changes differently from the path that the signal experiences [panel (b)]. A straightforward calculation shows that the pump picks up phase as $\phi_3 = \frac{2\pi n}{\lambda_3} Z$, where $n = 1.611$ is the refractive index of our LBO crystal [33] (since the crystal is phase-matched for degenerate SFG, this is the same for all three beams) and $\lambda_3 = 400$ nm. Similarly, the signal and idler acquire phase as $\phi_{1,2} = \frac{2\pi n}{\lambda_{1,2} \cos \theta} Z$, where $\lambda_{1,2} = 800$ nm.
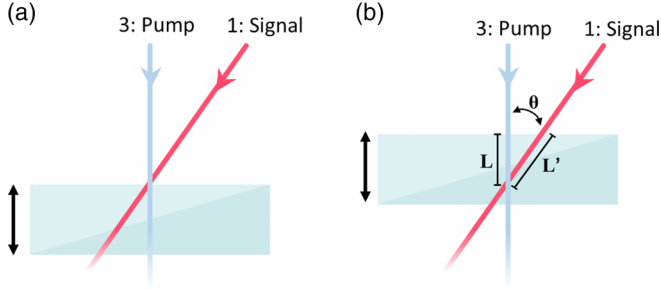
FIG. 4. Phase acquired during Z-scan. (a) At the start of the Z-scan of the crystal, the pump and signal beams intersect in front of the crystal. We set this to be a zero relative phase between the two beams. (b) As the crystal is translated through the intersection point, the optical path length for the pump beam L changes slower than the optical path of the signal beam L'. Thus as the crystal is translated through the intersection point, the relative phase is also scanned.

2. Classical model

In classical nonlinear optics, the central object is the nonlinear polarization, which describes the coupling of the incident light fields to a nonlinear medium, which gives rise to reemission of light at potentially different frequencies. For example, two fields at frequencies ω_1 and ω_2 can excite a nonlinear polarization associated with either sum-frequency generation $P(\omega_1 + \omega_2) = 2\epsilon_o \chi^{(2)} E_1 E_2$ or difference-frequency generation $P(\omega_1 - \omega_2) = 2\epsilon_o \chi^{(2)} E_1 E_2^*$, where E_1 and E_2 are the incident fields. Notice that any phase between fields E_1 and E_2 becomes a global phase on the polarization. Hence, processes with only two input fields are independent of this phase. If, however, three fields are incident, as is the case for our experiment, the relative phase between the three beams is no longer global. Hence, the phase can, in general, affect the nonlinear generation. To see this, consider three fields E_1, E_2, and E_3, the first two at a frequency ω, and the third at 2ω, that are incident in a $\chi^{(2)}$ nonlinear medium that is phase-matched for both SFG between E_1 and E_2, and DFG between both E_1 and E_3, and E_2 and E_3. In this case, the polarization will be

$$2\epsilon_o \chi^{(2)} (E_3 E_1^* e^{i(\phi_3 - \phi_1)} + E_3 E_2^* e^{i(\phi_3 - \phi_2)} + E_1 E_2 e^{i(\phi_2 + \phi_1)}). \quad (A1)$$

Here we have explicitly separated the phases ϕ_1, ϕ_2, and ϕ_3 from their respective fields to stress the phase dependence.

To solve for the generated fields with three incident beams, we use the so-called coupled wave equations, as described in Ref. [34],

$$\frac{dE_1}{dz} = \frac{2id_{\mathrm{eff}}\omega_1^2}{k_1 c^2} E_3 E_2^* e^{-i\Delta kz}, \quad (A2)$$

$$\frac{dE_2}{dz} = \frac{2id_{\mathrm{eff}}\omega_2^2}{k_2 c^2} E_3 E_1^* e^{-i\Delta kz}, \quad (A3)$$

$$\frac{dE_3}{dz} = \frac{2id_{\mathrm{eff}}\omega_3^2}{k_3 c^2} E_1 E_2 e^{-i\Delta kz}. \quad (A4)$$

In these equations, Δk is the phase mismatch, which we will set to 0 for our simple model, d_{eff} is the nonlinear strength

of the crystal, and k_i is the wave vector of each field. Setting $g = \frac{2d_{\mathrm{eff}}\omega_1}{c}$ and $\omega_1 = \omega_2 = \frac{1}{2}\omega_3$, we arrive at Eqs. (7)–(9) of the main text, which can be solved numerically.

Then to compute a value for the Sorkin parameter κ, we simply solve these equations under different initial conditions to compute each term of κ in Eq. (3) in the main text. For example, to compute P_{12}, we use the initial conditions $E_1(z = 0) \propto \sqrt{\mathcal{P}_1}$, $E_2(z = 0) \propto \sqrt{\mathcal{P}_2}$, and $E_3(z = 0) = 0$, where $\mathcal{P}_i$ is the power input into mode i. Then we evaluate the field in mode 3 (the pump mode) at $z = 1$ mm (the length of the crystal) to compute the optical power in mode 3 after exiting the crystal. While this is sufficient to show a nonzero value of κ, to model our experiment we include additional experiment factors: (i) the changing efficiency of the nonlinear processes during the z-scan and the different relative efficiencies of the three nonlinear processes, and (ii) the optical phase induced during the z-scan.

To model varying efficiencies, we first use a different coupling constant for each differential equation:

$$\frac{dE_1}{dz} = ig_1(Z)E_3 E_2^*, \quad (A5)$$

$$\frac{dE_2}{dz} = ig_2(Z)E_3 E_1^*, \quad (A6)$$

$$\frac{dE_3}{dz} = i2g_3(Z)E_1 E_2, \quad (A7)$$

and we also make them depend on the crystal position Z. We use different coupling constants to model the fact that, say, beams 1 and 2 may spatially and temporally overlap differently from beams 2 and 3. Then we numerically solve these equations for different values of Z. In particular, we assume a Gaussian form for $g_i(Z)$, defined in Eq. (13). where Δ characterizes the interaction range, g is a coupling constant defined below Eqs. (7)–(9), and η_i is a fitting parameter we use to account for experimental imperfections such as beam overlap and walk-off in the crystal.

The goal of this is to model the different interactions between the three beams as the crystal is translated through the focus. Experimentally, this effect is evident in different data sets. For example, the data presented in Fig. 8 show that as the crystal is moved through the intersection points of the beams, the different processes respond differently. We believe that this is caused by slightly different intersection angles between the three beams, and by the fact that the crystal is not perfectly perpendicular to the pump beam or the direction the crystal is moved.

To fit to our data, we observe the power in the pump mode 3 when all pairs of beams are turned on and the crystal is scanned through the focus. In particular, we measure the Z-dependence of $\mathcal{P}_{13}$ [Fig. 5(a)], $\mathcal{P}_{23}$ [Fig. 5(b)], and $\mathcal{P}_{12}$ [Fig. 5(c)]. For these sets of measurements, the input power in each beam is 870 mW in the signal (mode 1), 600 mW in the idler (mode 2), and 345 mW in the pump (mode 3). For our simulation, we then convert these average powers to fields, assuming Gaussian pulses with a width of $\tau = 140$ fs, a repetition rate of $R = 76$ MHz, and a beam diameter at the
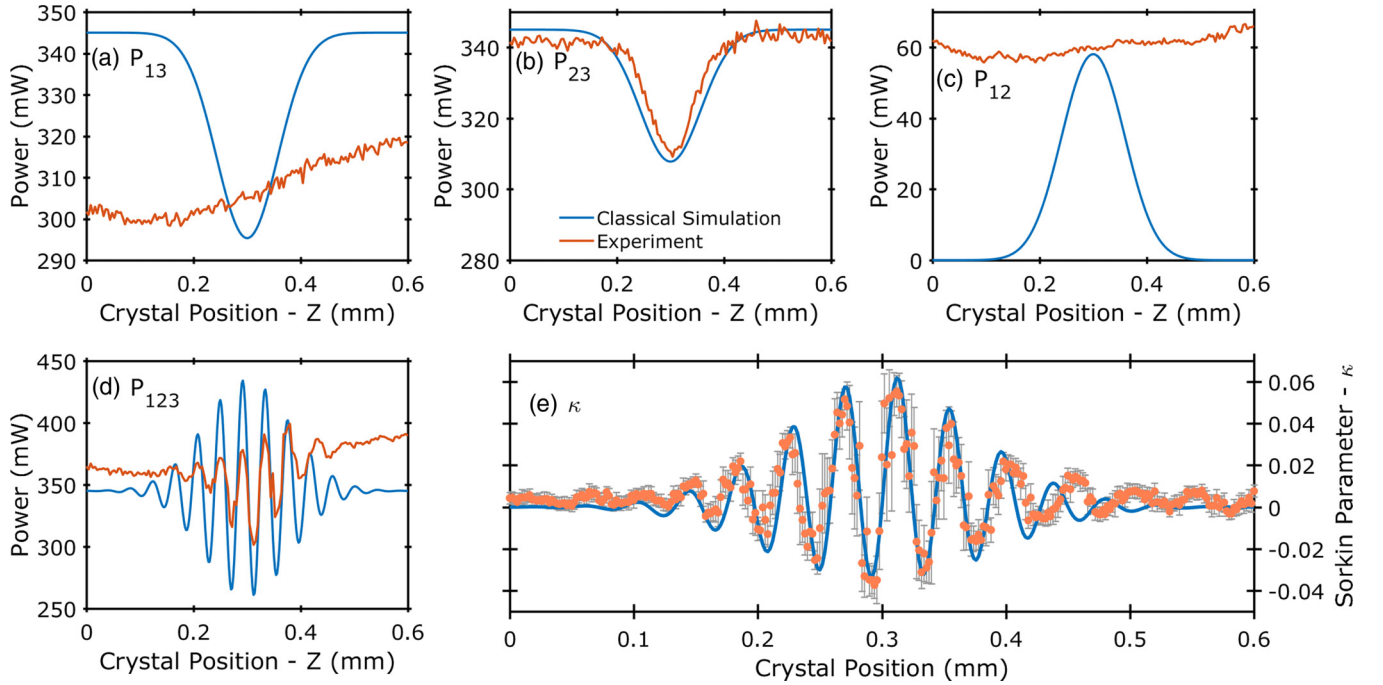
FIG. 5. Individual Sorkin terms vs the position of the crystal. The orange data show the power that is measured in the pump mode 3 after the crystal, while the blue curves are the results of classical simulations used to fit to the data. For the data in panels (a) ($\mathcal{P}_{13}$) and (b) ($\mathcal{P}_{23}$), the pump beam undergoes difference-frequency generation with the signal and idler, respectively. The decrease in power corresponds to difference-frequency power being generated into the third mode. (c) Sum-frequency generation between the signal and idler into the pump mode ($\mathcal{P}_{12}$). Over the range the crystal is scanned here, the power is more or less constant. (The data presented in Fig. 5, SFG-P_{12}, show that the SFG process eventually turns off.) (d) For these data, all three beams are open and the three processes all occur simultaneously, $\mathcal{P}_{123}$. The oscillations are induced by a phase discussed in the main text. For simplicity, we fix the width of the interaction region in our simulation to the narrowest process shown in panel (b). This is why the simulations presented in panels (a) and (c) only match the measured values at the focus. If instead we use longer interaction widths for the other two processes, our simulations predict that oscillations in panel (d) persist over a much longer range. This arises from phase-dependent interference from the vanishingly small tails of the Gaussian envelope function of the narrow process in panel (a).

focus of $w = 26\ \mu$m. Then the field is

$$E = \sqrt{\left(\frac{\ln 2}{\pi}\right)^{3/2} \frac{16}{R\tau w^2 \epsilon_0 c} \mathcal{P}}, \tag{A8}$$

where ϵ_0 is the permittivity of free space and c is the speed of light [31]. In our simulation, we set the initial conditions to match the experimental configuration (one beam blocked and the other two open), and then we adjust η_i to match the change in power observed throughout the z-scan. The result of these fits is shown in Figs. 5(a)–5(c). For simplicity, we assume the same interaction length for all three processes, $\Delta = 0.08$ mm, which is given by the narrowest process, which is DFG between the idler [Fig. 5(b)]. We set $\eta_1 = \eta_2 = 0.15$ and $\eta_3 = 0.05$, and we use $d_{\mathrm{eff}} = 0.749$ pm/V (given by [33] for LBO) to evaluate g. Additionally, we scale all three values of η by an additional factor of 0.3 when all three beams are open—i.e., when measuring $\mathcal{P}_{123}$—to account for the reduced "mutual overlap" between all three beams.

Finally, we add the Z-dependent phases (introduced in the previous section) to each of the respective fields. With all this in place, we compute the Sorkin parameter using our classical model. The result, plotted in Fig. 5(e), agrees well with our experimentally measured Sorkin parameter [plotted as the orange circles in Fig. 5(e)].

3. Quantum-mechanical description

To express our experiment within quantum mechanics, we start with the Hamiltonian $\hat{H}$ describing three modes interacting in a $\chi^{(2)}$-nonlinear medium:

$$\begin{aligned} \hat{H} &= \hbar\omega \hat{a}_1^\dagger \hat{a}_1 + \hbar\omega \hat{a}_2^\dagger \hat{a}_2 + 2\hbar\omega \hat{a}_3^\dagger \hat{a}_3 \\ &\quad + i\hbar\chi^{(2)}(\hat{a}_1 \hat{a}_2 \hat{a}_3^\dagger - \hat{a}_1^\dagger \hat{a}_2^\dagger \hat{a}_3). \end{aligned} \tag{A9}$$

Here, $\hat{a}_i^\dagger$ and $\hat{a}_i$ are the ladder operators acting on mode i. As in the main text, mode 1 describes the signal beam at frequency ω, mode 2 the idler beam at ω, and mode 3 the pump beam at 2ω. Since we measure photons in mode 3 after the interaction, we need to evolve the number operator associated with mode 3 as

$$\hat{n}_{3,f} = e^{i\hat{H}\tau/\hbar} \hat{a}_3^\dagger \hat{a}_3 e^{-i\hat{H}\tau/\hbar}. \tag{A10}$$

Here, τ, the interaction time, is proportional to the crystal length. We then apply a Baker-Campbell-Haussdorff expansion [32] up to fourth order to Eq. (A10). Given the number of terms in the expansion, we do not include the result here, but it is available in our MATHEMATICA script uploaded to [30]. Since we will only consider coherent input states $|\alpha_i\rangle$, we can
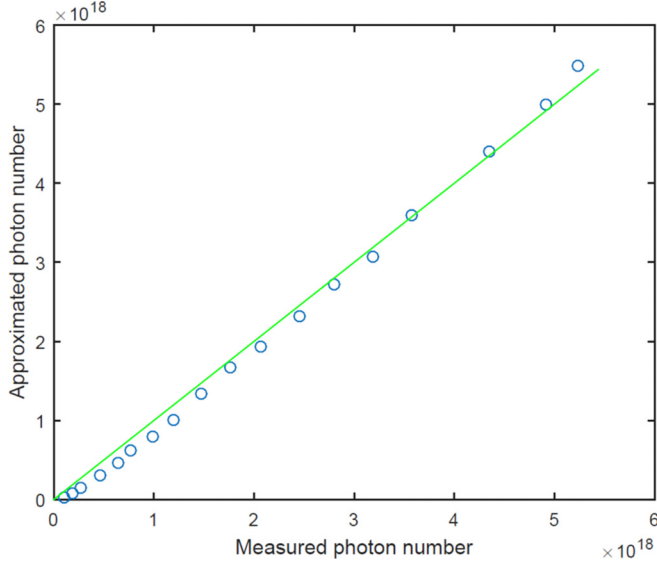
FIG. 6. Extraction of the nonlinear interaction Γ from measured data. The blue points are a plot of the approximated photon numbers vs the measured photon numbers. Note that we measure the average power and then compute the photon number per second. Error bars are not plotted, since the uncertainty is on the order of the size of the circles. For an ideal approximation, this procedure should result in a line with a slope of 1 (the green line).

do the following substitution into our expanded form of $\hat{n}_{3,f}$:

$$\hat{a}_i|\alpha_i\rangle \to \sqrt{n_i}\, e^{i\phi_i},$$
$$\langle\alpha_i|\hat{a}_i^\dagger \to \sqrt{n_i}\, e^{-i\phi_i}, \tag{A11}$$

where the phase factors ϕ_i represent the phase acquired during the Z-scan, and they are defined in the previous section. We are now interested in the average photon number in mode 3

after the interaction. This is computed by taking the expectation value of $\hat{n}_{3,f}$ for coherent inputs as

$$\langle\alpha_1,\alpha_2,\alpha_3|\,\hat{n}_{3,f}|\alpha_1,\alpha_2,\alpha_3\rangle$$
$$= f(\tau,\kappa(Z),n_1,n_2,n_3,\phi_1(Z),\phi_2(Z),\phi_3(Z)). \tag{A12}$$

From this equation, we compute the outcome photon number for all experimental configurations by inserting the specific states for α_i. For example, if all three beams are open, the outcome photon number in mode 3 is simply

$$n_{123} = \langle\alpha_1,\alpha_2,\alpha_3|\hat{n}_{3,f}|\alpha_1,\alpha_2,\alpha_3\rangle. \tag{A13}$$

If, e.g., the pump beam is blocked, the output photon number is

$$n_{12} = \langle\alpha_1,\alpha_2,0|\hat{n}_{3,f}|\alpha_1,\alpha_2,0\rangle, \tag{A14}$$

and so forth. As in the classical simulations, the relative phase cancels out for all configurations except n_{123} and has the same form as stated above. From the output photon numbers, we then compute the individual terms of Eq. (3) by normalizing by the input photon number. For example, $P_{12} = n_{12}/(|\alpha_1|^2 + |\alpha_2|^2 + |\alpha_3|^2)$, and so on. All of the necessary expectation values are defined in the MATHEMATICA code, available at [30].

From these normalized expectation values, we can construct the Sorkin parameter, defined in Eq. (3), resulting in the following expression:

$$\kappa = \frac{4}{3}\tau\chi^{(2)}\sqrt{n_1 n_2 n_3}\left(\frac{3}{2} - (\tau\chi^{(2)})^2(1 - n_1 - n_2 + n_3)\right)$$
$$\times \cos(\phi_1 + \phi_2 - \phi_3) + (\tau\chi^{(2)})^4 n_1 n_2 n_3$$
$$\times (2 + \cos(2\phi_1 + 2\phi_2 - 2\phi_3)). \tag{A15}$$

Given that the typical average powers in our experiment are ≈ 500 mW and we use a 76 MHz pump laser, we have approximately 10^{10} photons per pulse, hence $n_i \approx 10^{10}$. Furthermore, in the next section we estimate the maximum value
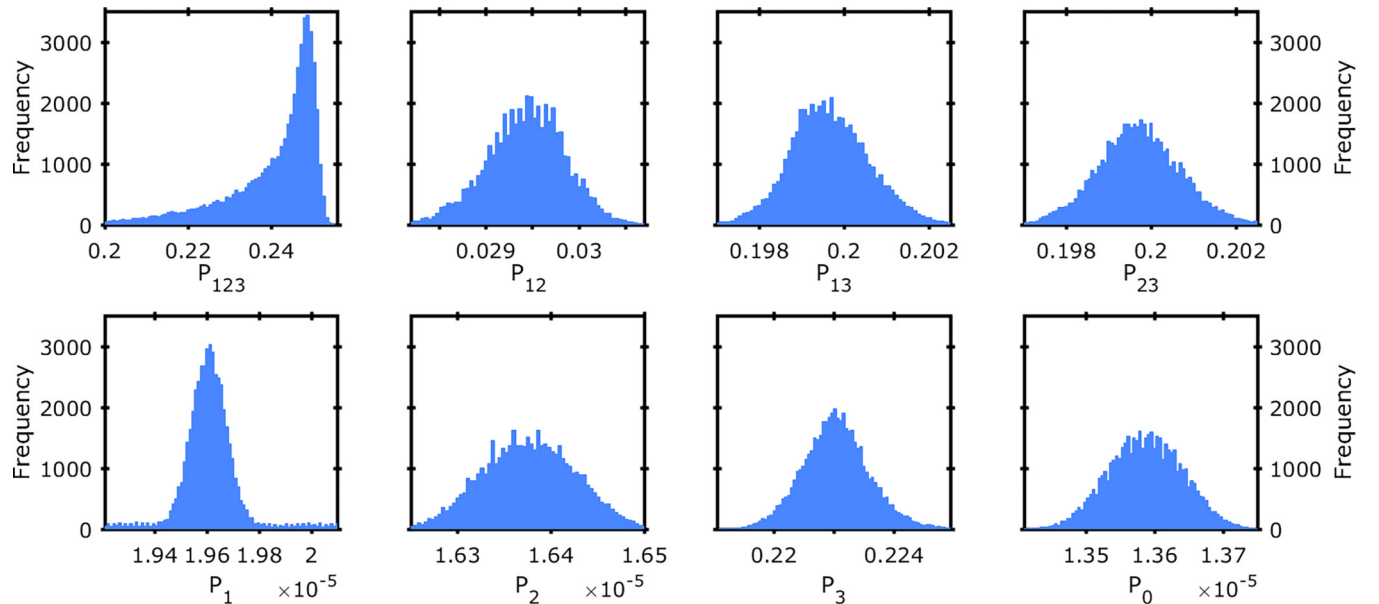

FIG. 7. Histograms of the individual terms of the Sorkin-parameter. The x-axis for these data is the normalized power, as described in the main text, for a given configuration of the experiment. For example, P_{12} is the normalized power measured when beams 1 and 2 are opened, and beam 3 is blocked. These data were used to compute the final value of $\kappa = 0.0334 \pm 0.0002$, the data presented in Fig. 3.
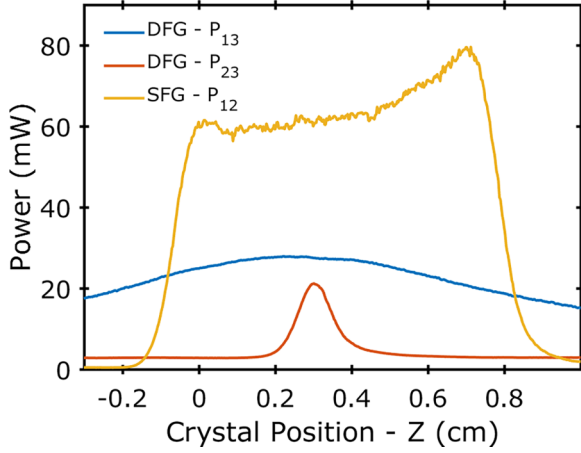
FIG. 8. Generated power for each two-mode process. For these data, one path is blocked and a detector is placed after the crystal in the blocked path. In other words, the detector is moved among the modes to ensure that the power generated by the nonlinear mixing is always measured. Then the power is recorded as the crystal is translated through the beam's focus. From the vastly different Z dependence of these data, one can observe that the different pairs of beams have significantly different overlap within the crystal.

of $\tau \chi^{(2)} \approx 10^{-6}$. Given these values, we can further approximate the Sorkin parameter in our nonlinear triple slit as

$$\kappa \approx 2\tau \chi^{(2)} \sqrt{n_1 n_2 n_3} \cos(\phi_1 + \phi_2 - \phi_3). \tag{A16}$$

Finally, we will add in the dependence on the crystal position Z. First we define $\tau \chi^{(2)} = \Gamma e^{-\frac{Z^2}{2\Delta^2}}$ making the effective nonlinearity, $\tau \chi^{(2)}$, a function of Z to represent the overlap of the beams with the crystal (just as was done for the coupling constants in the classical simulations). Here Γ is the maximum value of the nonlinear strength, which we estimate in the next section. Finally, substituting in the expressions derived above for the phases, and approximating to small intersection angles, we arrive at

$$\kappa(Z) \approx 2\Gamma \sqrt{n_1 n_2 n_3} \, e^{-\frac{Z^2}{2\Delta^2}} \cos\left(\frac{2\pi n \theta^2}{\lambda_{1,2}} Z\right). \tag{A17}$$

4. Fitting to the nonlinear strength

To fit to our experimental data, we first estimate the product of the nonlinearity and the interaction time, which we define as $\Gamma = \tau \chi^{(2)}$. To do this, we examine two interacting beams in the crystal. In particular, we examine the SFG process by sending the signal and idler beams into our nonlinear crystal and measuring the sum-frequency light generated in the pump beam, as in the configuration n_{12}. We then vary the input powers and measure the output power. These powers are then all converted into photon numbers n_1, n_2, and $n_{3,f}$.

Under these conditions, the only unknown from Eq. (A14) is Γ. We then compute the residuals between the measured data points and the predictions of Eq. (A14). By minimizing the residuals over Γ, we obtain $\Gamma = 1.05 \times 10^{-6}$. In Fig. 6 our approximation is visualized by plotting the predictions of Eq. (A14) versus the measured power (blue points). Ideally this results in a line with a slope of 1 (green line). The close
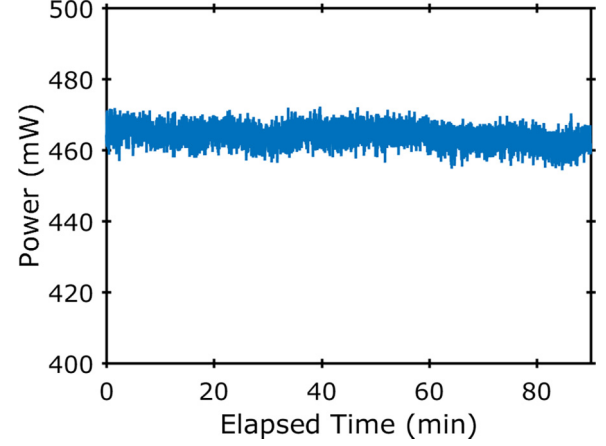

FIG. 9. Stability of $\mathcal{P}_{123}$. The power detected in the pump beam when all three beams are present plotted vs time. For these data, the crystal position was fixed and all three paths were left open. The phase in our experiment is stable for over 90 min.

fit demonstrates that we have sufficient precision using the fourth-order expansion.

Finally, to model the Z-scan of the crystal through the focus, we take Γ to be a Gaussian function of Z, as in Eq. (13). We then simply compute κ by computing the individual terms of Eq. (3) using Eq. (A12) for each crystal position Z where both Γ and the phase are functions of Z. The result, shown in the main text and discussed therein in more detail, agrees well with our experiment.

5. Additional measurements
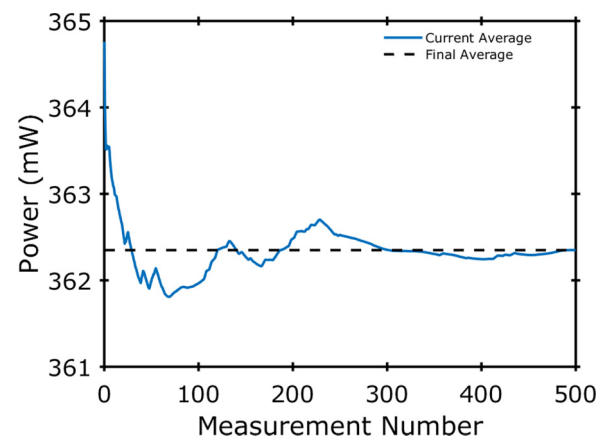
Figures 7–10 present additional measurements.

FIG. 10. Convergence of power measurements. For our measurements of κ, we measured the power 500 times to average out fast fluctuations. Here we plot typical results of the current average as a function of the measurement number as the blue curve. For these data, beams 1 and 3 were incident on the crystal, and the power was measured on beam 3 after the nonlinear interaction. The dashed black line shows the average of the full 500 data points. This shows that our measurements already begin to converge after ≈ 300 measurements.

[1] R. P. Feynman, R. B. Leighton, and M. L. Sands, *The Feynman Lectures on Physics: Quantum Mechanics*, The Feynman Lectures on Physics (Addison-Wesley, Reading, MA, 1965).

[2] R. D. Sorkin, Quantum mechanics as quantum measure theory, Mod. Phys. Lett. A **09**, 3119 (1994).

[3] U. Sinha, C. Couteau, T. Jennewein, R. Laflamme, and G. Weihs, Ruling out multi-order interference in quantum mechanics, Science **329**, 418 (2010).

[4] I. Söllner, B. Gschösser, P. Mai, B. Pressl, Z. Vörös, and G. Weihs, Testing born's rule in quantum mechanics for three mutually exclusive events, Found. Phys. **42**, 742 (2012).

[5] T. Kauten, R. Keil, T. Kaufmann, B. Pressl, Č. Brukner, and G. Weihs, Obtaining tight bounds on higher-order interferences with a 5-path interferometer, New J. Phys. **19**, 033017 (2017).

[6] M.-O. Pleinert, A. Rueda, E. Lutz, and J. von Zanthier, Testing Higher-Order Quantum Interference with Many-Particle States, Phys. Rev. Lett. **126**, 190401 (2021).

[7] D. Park, O. Moussa, and R. Laflamme, Three path interference using nuclear magnetic resonance: A test of the consistency of born's rule, New J. Phys. **14**, 113025 (2012).

[8] F. Jin, Y. Liu, J. Geng, P. Huang, W. Ma, M. Shi, C.-K. Duan, F. Shi, X. Rong, and J. Du, Experimental test of born's rule by inspecting third-order quantum interference on a single spin in solids, Phys. Rev. A **95**, 012107 (2017).

[9] A. R. Barnea, O. Cheshnovsky, and U. Even, Matter-wave diffraction approaching limits predicted by feynman path integrals for multipath interference, Phys. Rev. A **97**, 023601 (2018).

[10] J. P. Cotter, C. Brand, C. Knobloch, Y. Lilach, O. Cheshnovsky, and M. Arndt, In search of multipath interference using large molecules, Sci. Adv. **3**, e1602478 (2017).

[11] T. Vogl, H. Knopf, M. Weissflog, P. K. Lam, and F. Eilenberger, Sensitive single-photon test of extended quantum theory with two-dimensional hexagonal boron nitride, Phys. Rev. Res. **3**, 013296 (2021).

[12] S. Sadana, L. Maccone, and U. Sinha, Testing quantum foundations with quantum computers, Phys. Rev. Res. **4**, L022001 (2022).

[13] H. Yabuki, Feynman path integrals in the young double-slit experiment, Int. J. Theor. Phys. **25**, 159 (1986).

[14] H. De Raedt, K. Michielsen, and K. Hess, Analysis of multipath interference in three-slit experiments, Phys. Rev. A **85**, 012101 (2012).

[15] R. Sawant, J. Samuel, A. Sinha, S. Sinha, and U. Sinha, Nonclassical Paths in Quantum Interference Experiments, Phys. Rev. Lett. **113**, 120406 (2014).

[16] A. Sinha, A. H. Vijay, and U. Sinha, On the superposition principle in interference experiments, Sci. Rep. **5**, 10304 (2015).

[17] M.-O. Pleinert, J. von Zanthier, and E. Lutz, Many-particle interference to test born's rule, Phys. Rev. Res. **2**, 012051(R) (2020).

[18] S. Horvat and B. Dakić, Interference as an information-theoretic game, Quantum **5**, 404 (2021).

[19] L. A. Rozema, Z. Zhuo, T. Paterek, and B. Dakić, Higher-order interference between multiple quantum particles interacting nonlinearly, Phys. Rev. A **103**, 052204 (2021).

[20] O. S. Magana-Loaiza, I. De Leon, M. Mirhosseini, R. Fickler, A. Safari, U. Mick, B. McIntyre, P. Banzer, B. Rodenburg, G. Leuchs, and R. W. Boyd, Exotic looped trajectories of photons in three-slit interference, Nat. Commun. **7**, 13987 (2016).

[21] G. Rengaraj, U. Prathwiraj, S. N. Sahoo, R. Somashekhar, and U. Sinha, Measuring the deviation from the superposition principle in interference experiments, New J. Phys. **20**, 063049 (2018).

[22] K. Życzkowski, Quartic quantum theory: An extension of the standard quantum mechanics, J. Phys. A **41**, 355302 (2008).

[23] B. Dakić, T. Paterek, and Č. Brukner, Density cubes and higher-order interference theories, New J. Phys. **16**, 023028 (2014).

[24] C. M. Lee and J. H. Selby, Higher-order interference in extensions of quantum theory, Found. Phys. **47**, 89 (2017).

[25] T. Kauten, B. Pressl, T. Kaufmann, and G. Weihs, Measurement and modeling of the nonlinearity of photovoltaic and geiger-mode photodiodes, Rev. Sci. Instrum. **85**, 063102 (2014).

[26] K. S. Lee, Z. Zhuo, C. Couteau, D. Wilkowski, and T. Paterek, Atomic test of higher-order interference, Phys. Rev. A **101**, 052111 (2020).

[27] K.-H. Luo, M. Santandrea, M. Stefszky, J. Sperling, M. Massaro, A. Ferreri, P. R. Sharapova, H. Herrmann, and C. Silberhorn, Quantum optical coherence: From linear to nonlinear interferometers, Phys. Rev. A **104**, 043707 (2021).

[28] Z. Y. Ou, L. J. Wang, X. Y. Zou, and L. Mandel, Coherence in two-photon down-conversion induced by a laser, Phys. Rev. A **41**, 1597 (1990).

[29] L. J. Wang, X. Y. Zou, and L. Mandel, Observation of induced coherence in two-photon downconversion, J. Opt. Soc. Am. B **8**, 978 (1991).

[30] P. Namdar, P. K. Jenke, I. Alonso Calafell, A. Trenti, M. Radonjic, B. Dakic, P. Walther, and L. A. Rozema, Raw data for the manuscript "Experimental Higher-order Interference in a Nonlinear Triple Slit," Zenodo (2021).

[31] I. A. Calafell, L. A. Rozema, D. A. Iranzo, A. Trenti, P. K. Jenke, J. D. Cox, A. Kumar, H. Bieliaiev, S. Nanot, C. Peng *et al.*, Giant enhancement of third-harmonic generation in graphene–metal heterostructures, Nat. Nanotechnol. **16**, 318 (2021).

[32] J. J. Sakurai, *Modern Quantum Mechanics*, revised ed. (Addison-Wesley, Reading, MA, 1994).

[33] As Photonics, SNLO v.75, 08/10/2020, https://as-photonics.com/ (2020).

[34] R. W. Boyd, *Nonlinear Optics* (Academic Press, Burlington, MA, 2020).